ResearchGate

See discussions, stats, and author profiles for this publication at: https://www.researchgate.net/publication/41102552

Enhancement of cell radiation sensitivity by pegylated gold nanoparticles

Article *in* Physics in Medicine and Biology · February 2010

DOI: 10.1088/0031-9155/55/4/002 · Source: PubMed

CITATIONS
177

READS
276

14 authors, including:

Changhai Wang
Max Planck Institute for Chemical Physics of Solids
41 PUBLICATIONS **1,030** CITATIONS
SEE PROFILE

Hsianghsin Chen
Academia Sinica
51 PUBLICATIONS **632** CITATIONS
SEE PROFILE

Chia-Chi Chien
University of South Australia
46 PUBLICATIONS **891** CITATIONS
SEE PROFILE

Some of the authors of this publication are also working on these related projects:

Cervical cancer View project

Cancer Metabolism View project

All content following this page was uploaded by Ivan M Kempson on 16 May 2014.

The user has requested enhancement of the downloaded file.

Phys. Med. Biol. **55** (2010) 931–945 doi:10.1088/0031-9155/55/4/002

Enhancement of cell radiation sensitivity by pegylated gold nanoparticles

Chi-Jen Liu[1], Chang-Hai Wang[1], Shin-Tai Chen[1], Hsiang-Hsin Chen[1], Wei-Hua Leng[1], Chia-Chi Chien[1,2], Cheng-Liang Wang[1], Ivan M Kempson[1,3], YHwu[1,2,4,9], Tsung-Ching Lai[5], Michael Hsiao[5], Chung-Shi Yang[6], Yu-Jen Chen[7] and G Margaritondo[8]

[1] Institute of Physics, Academia Sinica, Nankang, Taipei 11529, Taiwan, Republic of China
[2] Department of Engineering and System Science, National Tsing Hua University, Hsinchu 30013, Taiwan, Republic of China
[3] Ian Wark Research Institute, University of South Australia, Mawson lakes, SA 5095, Australia
[4] Institute of Optoelectronic Sciences, National Taiwan Ocean University, Keelung 20224, Taiwan, Republic of China
[5] Genomics Research Center, Academia Sinica, Nankang, Taipei 11529, Taiwan, Republic of China
[6] Center for Nanomedicine, National Health Research Institutes, Miaoli 35053, Taiwan, Republic of China
[7] Mackay Memorial Hospital, Taipei 10449, Taiwan, Republic of China
[8] Ecole Polytechnique Fédérale de Lausanne (EPFL), CH-1015 Lausanne, Switzerland

E-mail: phhwu@sinica.edu.tw

Received 3 June 2009, in final form 13 November 2009
Published 20 January 2010
Online at stacks.iop.org/PMB/55/931

Abstract

Biocompatible Au nanoparticles with surfaces modified by PEG (polyethylene glycol) were developed in view of possible applications for the enhancement of radiotherapy. Such nanoparticles exhibit preferential deposition at tumor sites due to the enhanced permeation and retention (EPR) effect. Here, we systematically studied their effects on EMT-6 and CT26 cell survival rates during irradiation for a dose up to 10 Gy with a commercial biological irradiator ($E_{\text{average}} = 73$ keV), a Cu-Kα_1 x-ray source (8.048 keV), a monochromatized synchrotron source (6.5 keV), a radio-oncology linear accelerator (6 MeV) and a proton source (3 MeV). The percentage of surviving cells after irradiation was found to decrease by ∼2–45% in the presence of PEG-Au nanoparticles ([Au] = 400, 500 or 1000 μM). The cell survival rates decreased as a function of the dose for all sources and nanoparticle concentrations. These results could open the way to more effective cancer irradiation therapies by using nanoparticles with optimized surface treatment. Difficulties in applying MTT

[9] Author to whom any correspondence should be addressed.

 © 2010 Institute of Physics and Engineering in Medicine

assays were also brought to light, showing that this approach is not suitable for radiobiology.

(Some figures in this article are in colour only in the electronic version)

1. Introduction

The effectiveness of high-Z elements in enhancing cancer radiotherapy has been shown in previous reports (Matsudaira *et al* 1980, Mesa *et al* 1999, Herold *et al* 2000, Hainfeld *et al* 2004, Estève *et al* 2002). If such elements could be preferentially delivered to tumor sites, then the dose and the damage to healthy tissues could be reduced while preserving or enhancing the destructive effects for cancer.

Recently, preferential targeting of cancer areas by nanoparticles was achieved with the EPR (enhanced permeation and retention) effect (Matsumura and Maeda 1986). Besides being potentially useful for drug carrying in chemotherapy, EPR can improve radiotherapy: the nanoparticles can indeed trigger or enhance the effects of the radiation. These therapeutical opportunities motivated intense studies in the past decade (Paciotti *et al* 2004). Potentially, this approach could produce less adverse effects than conventional chemotherapy, is not affected by drug resistance and can reduce distant metastasis.

Radiotherapy by itself is already a leading choice for cancer treatment; therefore, its combination with nanomedicine appears as a feasible strategy (Hainfeld *et al* 2008). The combined approach would offer the same advantages as standard radiotherapy such as high penetration to go beyond the surface areas, plus the possibility of enhancing the killing effect with the presence of nanodrugs. The effectiveness of this approach primarily depends on the nanoparticle concentration in cancerous regions and the strong interaction with the irradiating beam.

In this context, gold—thanks to its strong absorption of radiation, notably x-rays—is an excellent candidate as nanoparticle constituent. It is also an inert and biocompatible element at the macro and μm size levels. However, the effects at the nanoparticle level cannot be automatically extrapolated from their bulk counterparts (Soto *et al* 2007, Chithrani *et al* 2006) and require detailed investigations with suitable experimental tools. In fact, there are extensive reports showing that Au nanoparticles have very high chemical activity due to their small sizes and surface defects (Wang and Ro 2006, Chiang *et al* 2006).

The EPR effect was previously demonstrated for small-size Au nanoparticles (Zhang *et al* 2009, Hainfeld *et al* 2006), and radiation response enhancement by Au nanoparticles was reported at the animal level (Hainfeld *et al* 2004). Au particles (1.5–3 μm) were studied for possible enhancement of the effects of hard x-rays and Cs-137 γ-rays (Herold *et al* 2000). While the killing by x-rays was significantly enhanced, in the case of γ-rays only a small increase was observed without clear statistical significance. No similar studies were previously performed at a cellular level or with nanometer-size particles.

In recent tests, we observed that Au nanoparticles with surfaces modified by PEG ('pegylated'), produced with an unconventional method based on intense x-ray irradiation, exhibited increased accumulation at tumor sites (unpublished data). This can lead to increased effectiveness in killing non-healthy cells.

However, the mere preferential concentration in cancerous areas with respect to normal tissues is not a sufficient condition for enhanced radiotherapy. Since the enhancement is

related to strong absorption, the concentration of nanoparticles in cancerous areas must be sufficiently high in absolute terms (e.g. 0.5–1 wt% Au resulted in a dose enhancement factor of ∼2 by using conventional 80–140 kVp x-ray tube sources (Hainfeld *et al* 2008)) and not just higher than in normal areas. Conversely, their concentration outside cancer regions must be low enough not to lead to excessive radiation damage.

The major cell killing phenomena in radiation therapy are DNA damage and the impact on cells of free radicals created by radiolysis. The first effect can be enhanced by the absorption increase, whereas the second can be augmented by the high chemical activity of Au nanoparticles. This could be due to an indirect cellular response induced by radiation such as oxidative stress (Singh *et al* 2009) or possibly due to the formation of free radicals which subsequently damage the cell DNA. These effects were not completely elucidated and are the subject of intense investigations.

In mouse tests, the required absolute concentration is difficult to achieve by intravenous injection of Au nanoparticles (Hainfeld *et al* 2004): more than 5 g kg^{-1} of nanoparticles were injected to achieve only a 5% increase in the effect of the cell irradiation. Furthermore, such nanoparticles can trigger an immune response leading to the excretion of most of them (Storm *et al* 1995, Davis 1997). Their concentration at tumor sites cannot be further increased by increasing the total injected amount without risking an adverse biological response even with a probably biocompatible, nanomaterial such as Au. Surface modification by PEG can assist in minimizing this problem (Otsuka *et al* 2003, Vlerken *et al* 2007, Oyewumi *et al* 2004). Furthermore, pegylation improves the Au nanosol stability reducing the problem of flocculation and aggregation (Wang *et al* 2008).

For therapy applications, the production method of the nanoparticle colloid must be simple, reliable and capable to guarantee high stability and strong concentrations. The aforementioned approach based on x-ray irradiation meets these requirements (Wang *et al* 2008). The irradiation-triggered process chemically produces Au nanoparticles from an AuCl solution and causes their surface pegylation. The process does not require any pre-added reducing agent, surfactant or template and it occurs in a single solution, making it easier to guarantee a clean and sterile synthesis environment for better biocompatibility.

The work described here constitutes the first step in establishing this new type of nanoparticle as an effective radiation enhancer for radiotherapy—by testing it with different irradiation sources at the cellular level before full-scale animal tests. The sources include x-ray emitters at different photon energies from 6.5 keV to 6 MeV—synchrotrons, a laboratory generator, an animal irradiator, an oncology linear accelerator—plus a proton emitter widely used for therapy.

Ultraviolet–visible (UV-VIS) absorption spectroscopy and dark-field visible light scattering microscopy were used to characterize the PEG-Au nanoparticle colloidal stability and real time dynamics. The overall results demonstrated excellent colloidal stability in different physiological environments. The Au nanosols were then introduced into EMT-6 and CT26 cell lines. Cell populations were then studied with and without the presence of pegylated Au nanoparticles, before and after irradiation with the aforementioned x-ray and proton sources.

Significant enhancement was measured with all types of radiation sources and cell lines—that can be directly attributed to the presence of the nanoparticles. The enhancement is far too large to be only explained by the nanoparticle-induced increase in the radiation absorption—thus indicating the presence of radiochemical effects also enhancing the cell killing.

2. Material and methods

2.1. Preparation of PEG-Au nanoparticle colloids

The colloids were synthesized from a mixed water (ultra-pure deionized Milli-Q water) solution with gold precursor (2 mM $HAuCl_4{\cdot}3H_2O$, Aldrich, MO, USA), NaOH (0.1 M, Showa Inc., Japan) and polyethylene glycol ('PEG', $HO–CH_2–(CH_3–O–CH_2)_n–CH_2–OH$, Showa Inc., Japan, molecular weight of 6000, 2 wt%). The precursor solution of 2 mM (Au concentration) was placed in polypropylene conical tubes (15 mL, Falcon®, Becton Dickinson, NJ) and bombarded with synchrotron x-rays at the BL01-A beam line of the NSRRC (National Synchrotron Radiation Research Center) storage ring (the photon energy distribution ranged from 8 to 15 keV and was centered at ∼12 keV (Hsu *et al* 2007)), and the dose was 10^5 Gy s^{-1} for 5 min, resulting in the formation of PEG-Au nanoparticles with 6.1 ± 1.9 nm diameter. The final concentration of the PEG-Au colloids was ∼75 mg mL^{-1}, as determined by induced coupled plasma optical emission spectrometry (ICP-OES, with a Perkin Elmer Optima 3000 DV, Perkin Elmer Co. Ltd, US instrument). Note that all the concentrations reported in this work were calibrated with ICP-OES measurements and therefore only refer to the pure Au concentration. A detailed description of this process was reported elsewhere including the purification procedure, the removal of unreacted PEG and gold salts and the concentration procedure (Wang *et al* 2007, 2008, Liu *et al* 2008). Our previous result clearly indicated that PEG chains are immobilized at the nanoparticle surfaces after x-ray exposure (Wang *et al* 2008).

The nature of the binding mechanism(s) and the resulting structure are currently unclear and additional tests are underway to identify them. Thiols are commonly used in binding to gold; therefore, when they are absent a physical mechanism is likely. We used PEG-Au nanoparticles' concentrations of 400, 500 and 1000 μM (Au concentration).

2.2. Colloidal stability examination

2.2.1. UV-VIS absorption spectra. The UV-VIS absorption spectra of the colloids were measured using a JASCO spectrophotometer (Model V-570, JASCO Inc., Japan) with a 1 cm quartz cuvette. This approach evaluates colloidal stability by monitoring the surface plasmon resonance (SPR) peak position and width that indicate flocculation (Wang *et al* 2007, 2009).

2.2.2. Dark field light scattering image. Dark-field visible light scattering microscopy was performed with an Olympus IX51 system with a CytoViva® (Aetos Technologies, Inc., Auburn, AL) modification. Microscopy was used to study the pristine state of nanoparticles from colloidal solutions in distilled dionized water, Hank's buffered salt solution (HBSS) and Dulbecco's Modified Eagle Medium and F12 (DMEMF-12, Gibco, Basel, Switzerland). A drop of PEG-Au or Au (10 nm, TED PELLA Inc., Redding, CA) nanoparticle solution was put on a glass slide, sealed with a cover slip and completed with objective oil (Olympus Inc.). The CytoViva system included a cardioid annular condenser producing high contrast, high signal-to-noise images, making it possible to observe the nanoparticle motion in the solution in real time—beating the diffraction limit (Wang *et al* 2009, Hasling 2006). This approach can detect nanoparticles as small as 20 nm using scattered light.

2.3. Cell culture

The cell lines included EMT-6 murine breast carcinoma cells and mice colorectal adenocarcinoma (CT26) cells (CRL-2638, ATCC, Rockville, MD). The cells were cultured in

DMEMF-12 Nutrient Mixture and Roswell Park Memorial Institute (RPMI, Gibco, Invitrogen Corp., Carlsbad, CA) medium, both containing 10% fetal bovine serum (FBS), 1% antibiotics (penicillin at 100 U mL^{-1} and streptomycin at 100 μg mL^{-1}) and L-glutamine at 37 °C in a humidified 5% CO_2 incubator.

2.4. Irradiation sources and dosimetry

Cell survival assays were performed after irradiation with the aforementioned sources and compared to control samples (i.e. cells not exposed to any PEG-Au or Au nanoparticles). All irradiation exposures were performed in air. Dose measurements used color dosimetry based on methylene blue (MB) bleaching as discussed by Liu *et al* (2009). Dose measurements based on MB are widely exploited for UV light but can also be applied to x-rays including very high flux levels up to at least 10^5 Gy s^{-1}. The cells were exposed to each radiation source after treatment with PEG-Au nanoparticles and compared to cells with no nanoparticle treatment.

2.4.1. RS 2000 x-ray biological irradiator. The RS 2000 x-ray biological irradiator (RadSource Tech. Inc., Boca Raton, FL) working at 160 kV and 25 mA with an average photon energy of ∼73 keV delivering a mean dose rate of 0.037 Gy s^{-1} was used. EMT-6 cells treated with 1 mL of 400 μM Au concentration PEG-Au nanoparticle solution mixed with cell culture medium (DMEMF-12) were exposed to individual total doses of 0.5, 1, 2, 4, 6, 8 and 10 Gy corresponding to irradiation times of 13.5, 27, 54, 108, 162, 216 and 270 s. Six different experimental tests were performed.

2.4.2. Laboratory-based Cu-Kα_1 x-ray facility. A Cu-Kα_1 (8.048 keV photon energy) x-ray source (in a Bruker D8 diffractomater, Germany) working at 45 kV and 40 mA, yielding a mean dose rate of 0.029 Gy s^{-1} was used. EMT-6 cells treated with 0.3 mL of 500 μM Au concentration PEG-Au nanoparticle solution mixed with cell culture medium (DMEMF-12) were exposed to individual total doses of 0.25, 1, 1.5, 2, 3 and 4 Gy corresponding to irradiation times of 8.6, 34.5, 51.7, 69, 103.4 and 137.9 s. Three different experimental tests were performed.

2.4.3. Synchrotron monochromatic x-rays. Monochromatic x-rays were produced with an energy of 6.5 keV, filtered by a Si(1 0 0) single-crystal wafer, at the BL01A beamline of NSRRC. Its evaluated mean dose rate was 0.26 Gy s^{-1}. EMT-6 cells treated with 0.1 mL of 500 μM Au concentration PEG-Au nanoparticle solution mixed with cell culture medium (DMEMF-12) were exposed to individual total doses of 1.5, 2.5 and 5 Gy corresponding to irradiation times of 5.7, 9.6 and 19.2 s. Two different experimental tests were performed.

2.4.4. Linear accelerator x-rays. A standard radio-oncology linear accelerator (Clinac IX, Varian Associates, Inc., Palo Alto, CA), operating at 6 MeV and yielding a mean dose rate of 0.04 Gy s^{-1}, was operated at the Mackay Memorial Hospital, Taiwan. CT26 cells were treated with 1 mL of 500 or 1000 μM Au concentration PEG-Au nanoparticle solution mixed with cell culture medium (RPMI). The cells were exposed to total doses of 0.5, 1, 2 and 3 Gy corresponding to irradiation times of 12.5, 5, 50 and 75 s and 3 different experimental tests were performed for each concentration.

2.4.5. Proton beam. A proton beam with a final potential of 3 MV (exit window) was produced with a NEC 9SDH-2 Tandem Pelletron Accelerator. The beam flux was 123 pA cm^{-2} s^{-1} at a 70 pA beam current and was used to treat EMT-6 cells with

0.1 mL of 500 μM Au concentration PEG-Au nanoparticle solution mixed with culture medium (DMEMF-12). Just before irradiation, the DMEMF-12 was discarded and the culture dish was fixed vertically in a special device to face the horizontal proton beam 1 cm from the exit window for the irradiation times of 1 and 3 s. Two different cell colonies were analyzed.

2.5. Radiobiology assays

2.5.1. MTT cell survival assay of Cu-Kα_1 irradiated cells. The MTT assay was performed for the Cu-Kα_1 exposed cells only to assess the cell survival rate. The MTT reagent (3-[4,5-dimethylthiazol-2-yl]-2,5-diphenyltetrazolium bromide; Thiazolyl blue, Sigma, Aldrich, USA) was dissolved in phosphate-buffered saline (PBS, pH 7.4) and filtered through a 0.22 μm filter. Before nanoparticle treatment, 850 EMT-6 cells/well were seeded in a 24-well culture dish. After seeding the cells for 24 h, PEG-Au nanoparticles (0.3 mL of 500 μM Au concentration solution) were introduced and kept for 48 h. Twenty-four hours after 60 s of x-ray irradiation, the MTT solution was added to each well and incubated for 3–4 h. Cellular reduction of MTT produced an insoluble, purple formazan.

At the end of the incubation period the formazan crystals were dissolved in dimethyl sulfoxide (DMSO) and the absorbance at 570 nm was measured with a standard micro plate reader (Sunrise, Tecan, Switzerland). The quantity of formazan crystals as measured by the absorbance at 570 nm is directly proportional to the number of living cells in the culture. The relative cell viability (%) was evaluated as $[A]_{\text{test}}/[A]_{\text{control}} \times 100$, where $[A]_{\text{test}}$ is the absorbance of the sample with PEG-Au nanoparticles and $[A]_{\text{control}}$ is that of the control sample without nanoparticles. Each experiment was performed three times.

2.5.2. Clonogenic cell survival assay. Clonogenic cell survival assays were performed for all irradiation methods. For the RS 2000 biological irradiator and linear accelerator irradiated cells, 100 EMT-6 cells/well were seeded and grown in a 6-well culture dish. For the laboratory-based Cu-Kα_1 x-ray and monochromatic synchrotron x-ray irradiation, 850 EMT-6 cells/well were seeded and grown in 48-well and 96-well culture dishes. Twenty-four hours after cell seeding, PEG-Au nanoparticles (400, 500 or 1000 μM Au concentration solution) were introduced and kept for a further 48 h before x-ray irradiation. After irradiation, the seeded cells were then detached by trypsin (0.5 g porcine trypsin and 0.2 g EDTA $\cdot$ 4Na per liter of HBSS) (Sigma, Saint Louis, MO). Subsequently, 100 EMT-6 cells/well of detached cells were seeded and grown in 6-well culture dishes and further incubated for 14 days. Finally, the cells were stained by 0.4% crystal violet and colonies were counted.

2.5.3. Analysis of DNA double-strand breaks. Immunohistochemistry was performed to determine the nuclear distribution of γ-H2AX in individual cells. 5000 EMT-6 cells were seeded on cover slides in a 24-well culture dish. After seeding the cells for 24 h, 500 μM Au concentration PEG-Au nanoparticles were introduced and kept for 48 h. Then the cells were irradiated with the RS 2000 x-ray biological irradiator (dose 2 Gy) or a laboratory-based Cu-Kα_1 x-ray source (dose again 2 Gy). The irradiated samples were further incubated for 60 min. One hour after each of the above-mentioned irradiations, the cells were fixed in 4% paraformaldehyde and permeabilized in a 0.1% solution of Triton X-100 in phosphate-buffered saline (PBS) for 10 min at room temperature. Subsequent detection was implemented after blocking in 5% FBS for 30 min at room temperature, using a 1:1000 dilution of the flourescein isothiocyanate (FITC)-labeled mouse monoclonal antibody against γ-H2AX (Millipore). Following overnight incubation at 4 $^{\circ}$C, the slides were washed three times with PBS. Then, the cover slips were counterstain with 4,6-diamidino-2-phenyindole (DAPI,

Vector Lab) and mounted on glass slides. The observation was performed by fluorescence microscopy (with the Olympus IX51 system).

2.6. Morphological study and fluorescence microscopy analysis of Cu-Kα_1 irradiated cells

Morphological studies were performed by optical microscopy. 850 EMT cells/well were seeded and grown in a 96-well dish. Forty-eight hours after cell seeding, the cells were irradiated by a Cu-Kα_1 (8.048 keV photon energy) x-ray source (in a Bruker D8 diffractomater, Germany) working at 45 kV and 40 mA. Twenty-four hours after this irradiation, the MTT solution was added to each well and incubated for 3–4 h. MTT-formazan crystals inside the cytoplasm produce a purple color that reveals the cell morphology. The cell morphology changes were observed by optical microscopy (using the Olympus IX 51 system, Japan, with a CCD camera) without any other treatment.

EMT cells were grown on a microscope glass slide overnight for complete adhesion and then irradiated by x-ray for 60 s (1.74 Gy) and cultured for 24 h more. The control group was treated with complete culture medium for 48 h without x-ray irradiation and the remnants of culture medium were washed out three times with PBS. The EMT-6 cells were fixed in PBS containing 4% paraformaldehyde and 2.5% glutaraldehyde and then blocked for 1 h at room temperature in PBS containing 5% bovine serum albumin (BSA). The mitochondria and cell skeleton were stained by Mito-R (red) and anti-mouse α-tubulin antibody (B512, Sigma) with the appropriate concentration in PBS containing 5% BSA for 1 h at room temperature and then washed three times with PBS. Secondary antibody, goat anti-mouse FITC conjugate, diluted 200 times in PBS was subsequently incubated with the samples for 1 h at room temperature. For locating the cell nucleus, the sample was incubated with the 4′,6-diamidino-2-phenylindole (DAPI) solution for several minutes and then rinsed with PBS. Finally, the samples were mounted in 80% glycerol mounting solution, placed onto a glass slide and sealed with a cover slip. The samples were imaged by fluorescence microscopy (once more with an Olympus IX51 system).

3. Results and discussion

3.1. Colloidal stability

Micrographs in figure 1 show individual PEG-Au particles in deionized water, HBSS and cell culture medium (DMEMF-12). This is in sharp contrast to the behavior of naked Au nanoparticle colloids that tend to aggregate in these media, as seen in figure 2. The UV-VIS absorption spectra, figures 1(d) and 2(d), confirm the PEG-Au colloidal stability. The SPR peak of PEG-Au remains unchanged in all three solutions while naked Au in HBSS and MDEMF-12 shift toward longer wavelengths and broadens, indicating aggregation. These results demonstrate excellent colloidal stability of the PEG-Au nanoparticles in different *in vitro* environments.

3.2. MTT assay of Cu-Kα_1 irradiated cells

This assay is a widely used method to assess cell growth potential based on mitochondria function measurements. However, it is not commonly used for cellular response to ionizing radiation, as discussed later.

Figure 3 shows optical images of control and viable cells, after Cu-Kα_1 x-ray irradiation for 60 s, reacted with the MTT reagent. The surviving cell number decreases significantly with respect to the non-irradiated control specimen. The surviving cells show abnormal

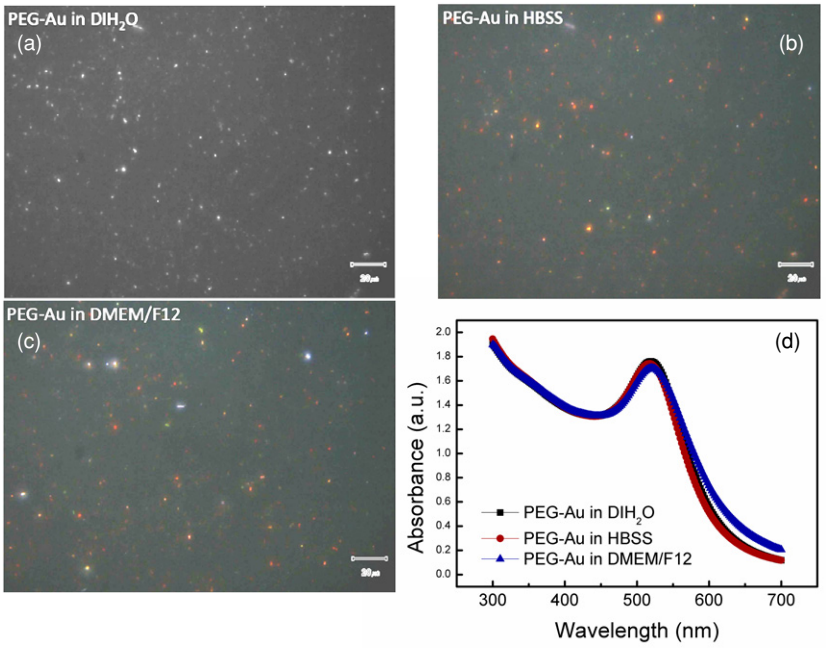

Figure 1. Colloidal stability test of Peg-Au nanoparticles by dark field images in (a) DI water (b) HBSS buffer solution (c) DMEM/F-12 medium; (d) UV-VIS absorption spectra for Peg-Au nanoparticles in the same conditions as above. Bar = 20 μm.

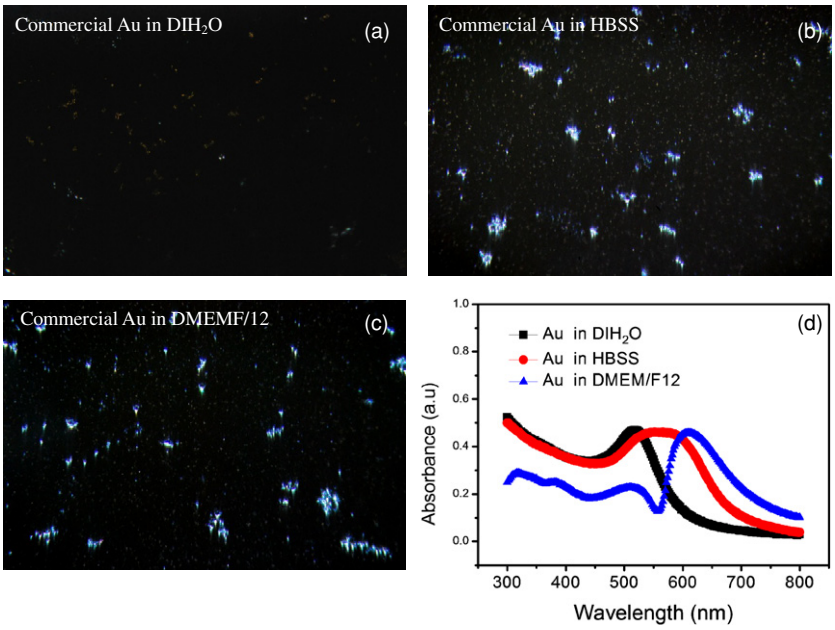

Figure 2. Colloidal stability test of commercial bare-Au nanoparticles by dark field images and UV-VIS absorption for the same systems as in figure 1.

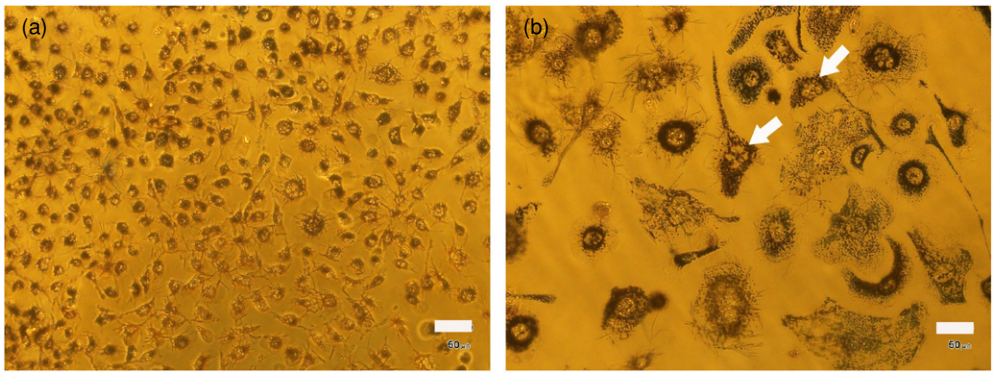

Figure 3. Optical images of EMT-6 cells reacted with the MTT reagent: (a) non-irradiated control specimen and (b) cells irradiated for 1.74 Gy with laboratory-based Cu Kα_1 x-rays. The arrows indicated the multiple nuclei in the irradiated cells. Bar = 50 μm.

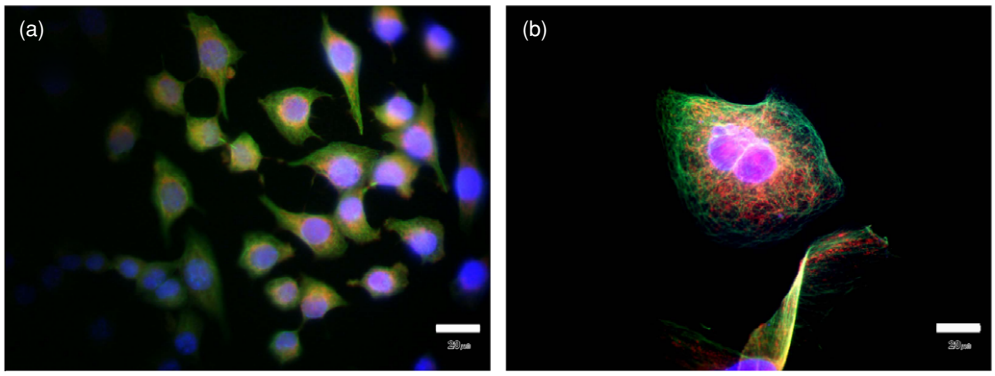

Figure 4. Fluorescence microimages of EMT-6 cells irradiated in the same systems as in figure 3: (a) non-irradiated control specimen and (b) specimen irradiated at the 1.74 Gy level with Cu Kα_1 x-rays. The mitochondria, cell skeleton and nucleus were stained by Mito-R (red), α-tubulin antibody (green) and DAPI (blue). Bar = 20 μm.

senescence morphology after irradiation: the cell size increased on the average 3–4 times. It was previously reported that after irradiation, cell cycles tend to stop or pause to repair the damaged DNA (Petrović *et al* 2006, Bernhard *et al* 1995). The surviving cells exhibited abnormal mitosis, developing multiple nuclei with much larger size (Ianzini and Mackey 1997, Mackey and Ianzini 2000, Eriksson *et al* 2007). This phenomenon was reported as a cause of cell death (Roninson *et al* 2001, Castedo *et al* 2004).

The number of mitochondria and the cytoskeleton within the cytoplasm of the surviving cells were determined by fluorescence microscopy, as shown, for example, in figure 4. More mitochondria and cytoskeleton were found in irradiated cells compared (figure 4(b)) to non-irradiated cells (figure 4(a)). MTT is reduced to purple formazen by the dehydrogenase enzymes in the mitochondria of living cells (Mosmann 1983, Liu *et al* 1997, Berridge and Tan 1993) and the production of formazan is proportional to the level of metabolic activity of cells. The increase in mitochondria induced by irradiation enhances the formation of formazen.

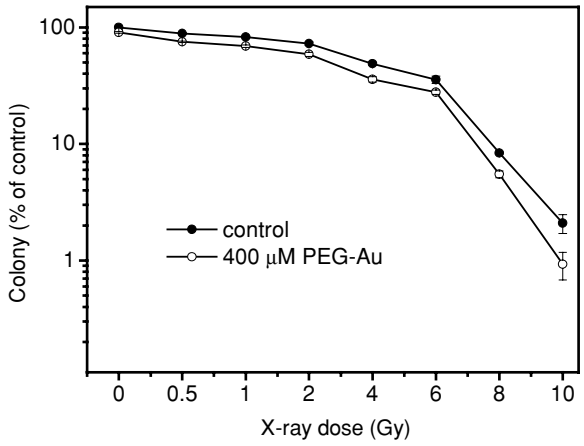

Figure 5. Survival rate versus dose for EMT-6 cells irradiated with the RS 2000 x-ray biological irradiator. The full dots refer to control cells whereas the open circles are for cells cultured in the presence of 400 μM Au concentration PEG-Au nanoparticles. The doses delivered to the cells were 0.5, 1, 2, 4, 6, 8 and 10 Gy. The data represent the mean $\pm$ standard deviation of the results from six independent experiments.

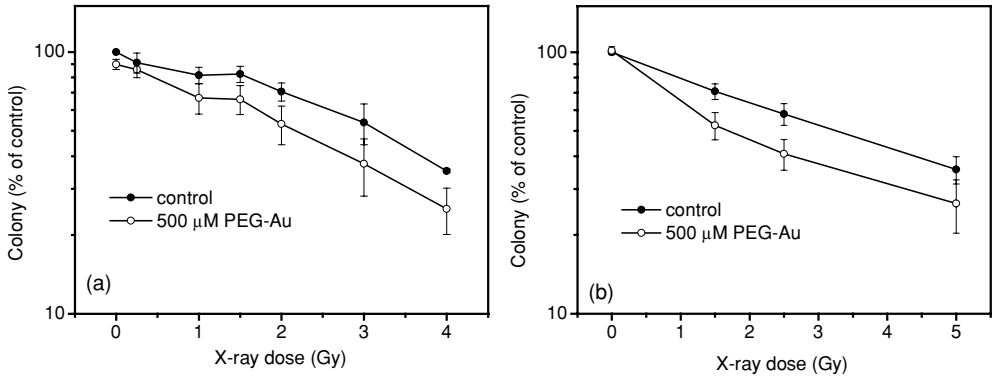

Figure 6. Survival rate versus dose for control and 500 μM Au concentration of PEG-Au-exposed EMT-6 cells irradiated by (A) Cu Kα_1 x-rays and (B) monochromatic synchrotron x-rays. The doses delivered to the cells were 0.25, 1, 1.5, 2, 3 and 4 Gy for Cu Kα_1 x-rays, as well as 1.5, 2.5 and 5 for monochromatic synchrotron x-rays. The data represent the average $\pm$ standard deviation of the results from three experiments with Cu Kα_1 x-rays and from two experiments with monochromatic synchrotron x-rays.

Therefore, the mitochondria in surviving cells alter the MTT assay quantification and can lead to misinterpretation of its results. The MTT assay is not suitable for the accurate measurement of the cellular response to radiation.

3.3. Clonogenic cell survival assays

3.3.1. X-ray irradiation. Cells were exposed to the RS 2000 x-ray biological irradiator for doses of 0.5, 1, 2, 4, 6, 8 and 10 Gy and subsequently assessed by their ability to proliferate,

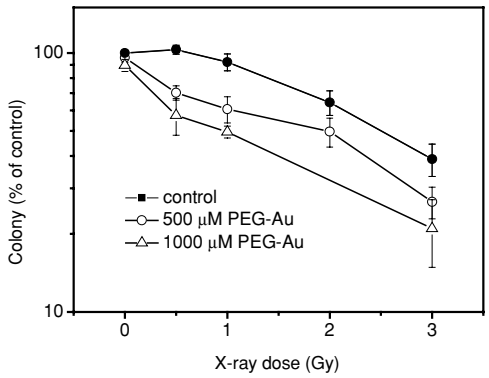

Figure 7. Survival rate versus dose for control and 500 μM and 1000 μM Au concentration of PEG-Au-exposed CT26 cells irradiated by x-rays emitted by the linear accelerator. The doses delivered to the cells were 0.5, 1, 2 and 3 Gy. The data represent the average $\pm$ standard deviation of the results from three independent experiments.

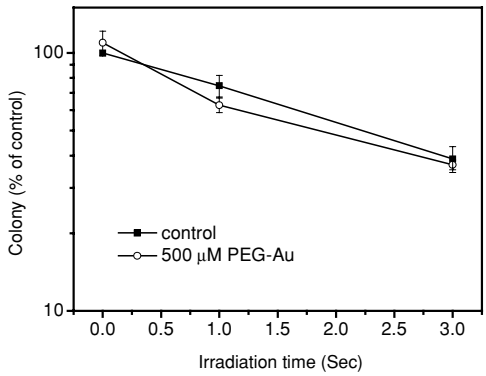

Figure 8. The effects of 500 μM Au concentration of PEG-Au exposure on the survival rate in the case of proton beam irradiation. The error bars reflect the difference in the averages measured for two different cell colonies.

estimated from colony conversion. Figure 5 shows the decrease in the fraction of viable cells with irradiation dose as well as the killing enhanced effect of exposure to PEG-Au nanoparticles. For example, after a dose of 1 or 2 Gy, the survival rate was 82.5% and 72.5% for the control cells and decreased to 69% and 58.7% respectively for cells exposed to PEG-Au nanoparticles. Similar decreases were found for all doses.

Similar trends were observed for all x-ray sources. PEG-treated Au enhanced the death rate of cells when irradiated with Cu-Kα_1, monochromatic synchrotron and linear accelerator produced x-rays (figures 6 and 7). Quantitatively, the radiation-induced survival rate decrease was 5.4–17.4%. Likewise, in the case of CT26 cell irradiation by x-rays emitted by a linear accelerator, the decrease was by 12.3–45.6%. The effect tended to increase with the colloidal concentration, consistent with our previous work (Liu *et al* 2008). Note that the ratio of the data with gold versus the control data does increase (or stays constant) as the dose increases.

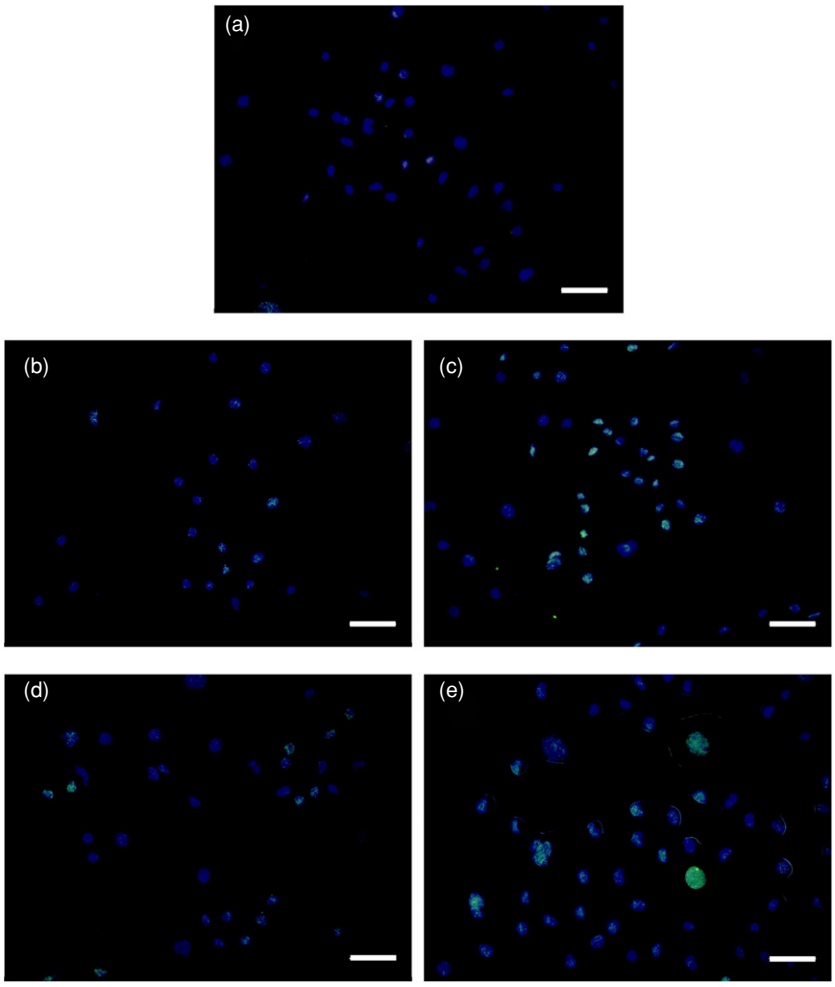

Figure 9. Immunohistochemistry of γ-H2AX in EMT-6 cells: (a) non-irradiated control specimen, and cell irradiated by Cu Kα_1 x-rays for 2 Gy cocultured (b) with no PEG-Au nanoparticles and (c) with 500 μM Au concentration PEG-Au nanoparticles; cell irradiated by RS 2000 x-ray biological irradiator for 2 Gy cocultured (d) with no PEG-Au nanoparticles and with (e) 500 μM Au concentration PEG-Au nanoparticles. The irradiated cells were incubated for 60 min after x-ray irradiation. The green and blue fluorescence indicated γ-H2AX (FITC) and nuclei (DAPI). Bar = 50 μm.

3.3.2. Proton beam irradiation. The viability results are shown in figure 8 and the effect of PEG-Au nanoparticles is similar to that for x-ray irradiation. The decrease in survival rate reached 2–11.9%.

These tests, therefore, demonstrated significantly enhanced radiation killing with the inclusion of PEG-Au colloids for various x-ray sources. The proton beam similar to those commonly used in proton therapy induced a weak but still detectable radiation enhancement effect. The selected x-ray sources deliver different intensities and photon energy distributions; they thus enabled us to establish the general character of the enhancement effect triggered by PEG-Au. The cell survival rate decreased by ~2–45%, depending on the type of radiation and

source. This is larger than the enhancement predicted by Cho with Monte Carlo simulations (Cho 2005) and provides additional evidence of other radiation effects that enhance cellular death.

The cause of this enhancement is in fact unclear. One could imagine that the mere increase of radiation absorption could be the explanation. But this is not reasonable since the PEG-Au concentration in cancer regions is far less than 1 wt%. An additional effect must be involved in which the PEG-Au nanoparticles are directly responsible for radiation-induced cell killing. The clarification and validation of this effect could be facilitated in future experiments by extending the dose range and the gold concentration range.

3.4. DNA double-strand breaks assay

DNA double-strand breaks (DSBs) analysis is commonly used for DNA damage induced by ionizing radiation and analyzes the treatment response to radiotherapy. Histone H2AX phosphorylation is the earliest biochemical process after DSB formation. Consequently, the phosphorylated domains of Histone H2AX can be detected by immunofluorescence as subnuclear domains, called γ-H2AX (Macphail *et al* 2003, Han *et al* 2006). We confirmed the enhanced x-ray damage caused by PEG-Au nanoparticles after irradiation by Cu Kα_1 x-rays or by the RS 2000 x-ray biological irradiator. Compared to cells without PEG-Au nanoparticle treatment (figures 9(b) and (a)), cells treated with 500 m Au concentration PEG-Au nanoparticles clearly exhibited the formation of γ-H2AX after the above-mentioned irradiations (figure 9(e)), indicating that PEG-Au nanoparticles enhance the DSBs. This result agrees with that of clonogenic cell survival assay and confirms the enhancement of irradiation-induced killing by PEG-Au nanoparticles.

4. Conclusions

Several aspects make these results interesting for possible therapy applications. The synthesis method based on x-ray irradiation is simple and reliable, yet capable to produce very stable and highly concentrated PEG-Au colloids with no reducing agents. Such PEG-Au nanoparticles were found to systematically increase cell mortality rate by different types of irradiation. This system is therefore promising and should be carefully analyzed as a potential enhancer for radiotherapy. The effects observed do not appear to be due only to an increase in localized radiation absorption. Investigations are underway to further clarify the underlying phenomena.

Acknowledgments

We wish to thank Dr Chia-Fu Chou for the CCD camera setup. This work is supported by the National Science and Technology Program for Nanoscience and Nanotechnology, the Thematic Research Project of Academia Sinica, the Biomedical Nano-Imaging Core Facility at National Synchrotron Radiation Research Center (Taiwan), the Center for Biomedical Imaging (CIBM) in Lausanne—partially funded by the Leenaards and Jeantet foundations—the Swiss Fonds National de la Recherche Scientifique and the EPFL.

References

Bernhard E J, Maity A, Muschel R J and McKenna W G 1995 Effects of ionizing radiation on cell cycle progression *Radiat. Environ. Biophys.* **34** 79–83

Berridge M V and Tan A S 1993 Characterization of the cellular reduction of 3-(4,5-dimethylthiazol-2-yl)-2,5-diphenyltetrazolium bromide (MTT): subcellular localization, substrate dependence, and involvement of mitochondrial electron transport in MTT reduction *Arch. Biochem. Biophys.* **303** 474–82

Castedo M, Perfettini J L, Roumier T, Andreau K, Medema R and Kroemer G 2004 Cell death by mitotic catastrophe: a molecular definition *Oncogene* **23** 2825–37

Chiang C W, Wang A and Mou C Y 2006 CO oxidation catalyzed by gold nanoparticles confined in mesoporous aluminosilicate Al-SBA-15: pretreatment methods *Catal. Today* **117** 220–7

Chithrani B D, Ghazani A A and Chan W C W 2006 Determining the size and shape dependence of gold nanoparticle uptake into mammalian cells *Nano Lett.* **6** 662–8

Cho S H 2005 Estimation of tumour dose enhancement due to gold nanoparticles during typical radiation treatments: a preliminary Monte Carlo study *Phys. Med. Biol.* **50** N163–73

Davis S S 1997 Biomedical applications of nanotechnology—implications for drug targeting and gene therapy *Trends Biotechnol.* **15** 217–24

Eriksson D, Löfroth P O, Johansson L, Riklund K A and Stigbrand T 2007 Cell cycle disturbances and mitotic catastrophes in HeLa Hep2 cells following 2.5 to 10 Gy of ionizing radiation *Clin. Cancer Res.* **15** 5501s–8s

Estève F, Corde S, Elleaume H, Adam J F, Joubert A, Charvet A M, Biston M C, Balosso J and Le Bas J F 2002 Enhanced radio sensitivity with iodinated contrast agents using monochromatic synchrotron x-rays on human cancerous cells *Acad. Radiol.* **9** S540–3

Hainfeld J F, Dilmanian F A, Slatkin D N and Smilowitz H M 2008 Radiotherapy enhancement with gold nanoparticles *J. Pharm. Pharmacol.* **60** 977–85

Hainfeld J F, Slatkin D N, Focella T M and Smilowitz H M 2006 Gold nanoparticles: a new x-ray contrast agent *Br. J. Radiol.* **79** 248–53

Hainfeld J F, Slatkin D N and Smilowitz H M 2004 The use of gold nanoparticles to enhance radiotherapy in mice *Phys. Med. Biol.* **49** N309–15

Han J, Hendzel M J and Allalunis-Turner J 2006 Quantitative analysis reveals asynchronous and more than DSB-associated histone H2AX phosphorylation after exposure to ionizing radiation *Radiat. Res.* **165** 283–92

Hasling T A 2006 Biomedical applications of nanotechnology—implications for drug targeting and gene therapy *Microsc. Today* **14** 22–6

Herold D M, Das I J, Stobbe C C, Iyer R V and Chapman J D 2000 Gold microspheres: a selective technique for producing biologically effective dose enhancement *Int. J. Radiat. Biol.* **76** 1357–64

Hsu P C *et al* 2007 Photosynthesis and structure of electroless Ni–P films by synchrotron x-ray irradiation *J. Vac. Sci. Technol.* A **25** 615–20

Ianzini F and Mackey M A 1997 Spontaneous premature chromosome condensation and mitotic catastrophe following irradiation of HeLa S3 cells *Int. J. Radiat. Biol.* **72** 409–21

Liu C J *et al* 2008 Enhanced x-ray irradiation-induced cancer cell damage by gold nanoparticles treated by a new synthesis method of polyethylene glycol modification *Nanotechnology* **19** 295014–5

Liu C J, Wang C H, Wang C L, Hwu Y, Lin C Y, Je J H and Margaritondo G 2009 Simple dose rate measurements for a very high synchrotron x-ray flux *J. Synchrotron Radiat.* **16** 395–7

Liu Y, Peterson D A, Kimura H and Schubert D 1997 Mechanism of cellular 3-(4,5-dimethylthiazol-2-yl)-2,5-diphenyltetrazolium bromide (MTT) reduction *J. Neurochem.* **69** 581–93

Mackey M A and Ianzini F 2000 Enhancement of radiation-induced mitotic catastrophe by moderate hyperthermia *Int. J. Radiat. Biol.* **76** 273–80

Macphail S H, Banath J P, Yu T Y, Chu E H M, Lambur H and Olive P L 2003 Expression of phosphorylated histone H2AX in cultured cell lines following exposure to x-rays *Int. J. Radiat. Biol.* **79** 351–8

Matsudaira H, Ueno A M and Furuno I 1980 Iodine contrast medium sensitizes cultured mammalian cells to x rays but not to γ rays *Radiat. Res.* **84** 144–8

Matsumura Y and Maeda H 1986 A new concept for macromolecular therapeutics in cancer chemotherapy: mechanism of tumoritropic accumulation of proteins and the antitumor agent smancs *Cancer Res.* **46** 6387–92

Mesa A V, Norman A, Solberg T D, Demarco J J and Smathers J B 1999 Dose distributions using kilovoltage x-rays and dose enhancement from iodine contrast agents *Phys. Med. Biol.* **44** 1955–68

Mosmann T 1983 Rapid colorimetric assay for cellular growth and survival: application to proliferation and cytotoxicity assays *J. Immunol. Methods* **65** 55–63

Otsuka H, Nagasaki Y and Kataoka K 2003 PEGylated nanoparticles for biological and pharmaceutical applications *Adv. Drug. Deliv. Rev.* **55** 403–19

Oyewumi M O, Yokel R A, Jay M, Coakley T and Mumper R J 2004 Comparison of cell uptake, biodistribution and tumor retention of folate-coated and PEG-coated gadolinium nanoparticles in tumor-bearing mice *J. Control. Release* **95** 613–26

Paciotti G F, Myer L, Weinreich D, Goia D, Pavel N, McLaughlin R E and Tamarkin L 2004 Colloidal gold: a novel nanoparticle vector for tumor directed drug delivery *Drug Deliv.* **11** 169–83

Petrović I, Ristić-Fira A, Todorović D, Valastro L, Cirrone P and Cuttone G 2006 Radiobiological analysis of human melanoma cells on the 62 MeV CATANA proton beam *Int. J. Radiat. Biol.* **82** 251–65

Roninson I B, Broude E V and Chang B D 2001 If not apoptosis, then what? Treatment-induced senescence and mitotic catastrophe in tumor cells *Drug Resist. Update* **4** 303–13

Singh S P, Hader D P and Sinha R P 2009 Cyanobacteria and ultraviolet radiation (UVR) stress: mitigation strategies *Ageing Res. Rev.* at press (doi:10.1016/j.arr.2009.05.004)

Soto K, Garza K M and Murr L E 2007 Cytotoxic effects of aggregated nanomaterials *Acta Biomater* **3** 351–8

Storm G, Belliot S O, Daemen T and Lasic D D 1995 Surface modification of nanoparticles to oppose uptake by the mononuclear phagocyte system *Adv. Drug. Deliv. Rev.* **17** 31–48

Vlerken L E V, Vyas T K and Amiji M M 2007 Poly(ethylene glycol)-modified nanocarriers for tumor-targeted and intracellular delivery *Pharm. Res.* **24** 1405–14

Wang C H *et al* 2007 Aqueous gold nanosols stabilized by electrostatic protection generated by x-ray irradiation assisted radical reduction *Mater. Chem. Phys.* **106** 323–9

Wang C H *et al* 2008 Optimizing the size and surface properties of polyethylene glycol (PEG)–gold nanoparticles by intense x-ray irradiation *J. Phys. D: Appl. Phys.* **41** 195301–8

Wang C H *et al* 2009 Intense x-ray induced formation of silver nanoparticles stabilized by biocompatible polymers *Appl. Phys.* A **97** 295–300

Wang C T and Ro S H 2006 Surface nature of nanoparticle gold/iron oxide aerogel catalysts *J. Non-Cryst. Solids* **352** 35–43

Zhang G, Yang Z, Lu W, Zhang R, Huang Q, Tian M, Li L, Liang D and Li C 2009 Influence of anchoring ligands and particle size on the colloidal stability and*in vivo* biodistribution of polyethylene glycol-coated gold nanoparticles in tumor-xenografted mice *Biomaterials* **30** 1928–36

View publication stats